Received: 19 October 2017 | Revised: 20 March 2018 | Accepted: 21 March 2018

DOI: 10.1002/cne.24452

RESEARCH ARTICLE

WILEY JCN RESEARCH IN SYSTEMS NEUROSCIENCE THE JOURNAL OF COMPARATIVE NEUROLOGY

# Myelination of the developing lateral olfactory tract and anterior commissure

L. N. Collins | D. L. Hill | P. C. Brunjes

Department Psychology, University of Virginia, Charlottesville, Virginia

**Correspondence**
P. C. Brunjes, Department Psychology, University of Virginia, 102 Gilmer Hall, 400400, Charlottesville, VA 22904-4400.
Email: brunjes@virginia.edu

**Funding information**
NIH, Grant/Award Number: DC000338; NIDCD, Grant/Award Number: DC00407

## Abstract

Both the lateral olfactory tract (LOT) and anterior limb of the anterior commissure (AC) carry olfactory information. The LOT forms the projection from the olfactory bulb to the ipsilateral olfactory cortices, while the AC carries odor information across the midline to the contralateral olfactory cortex and bulb. The LOT and AC differ on a number of dimensions, including early development and functional onset. The present work, examining their myelination in mice, reveals additional important differences. For example, the LOT initiates myelination 3–4 days earlier than the AC, evidenced by both an earlier increase in myelin basic protein staining seen with immunohistochemistry and an earlier appearance of myelinated fibers using electron microscopy. While both exhibit a period of rapid myelination, it occurs 4–5 days earlier in the LOT than the AC. The tracts also respond differently to early sensory restriction. Unilateral naris occlusion from the day after birth to postnatal day 30 had no consistent effects on the AC but resulted in significantly thinner myelin sheaths relative to axon caliber in the LOT. Finally, the two tracts differ structurally (the LOT contains larger, more densely packed axons with significantly thicker myelin sheaths resulting in a conduction velocity that is more than twice as fast as the AC). The findings indicate that these two large, accessible tracts provide an important means for studying brain maturation due to basic differences in both the timing of their maturation and general organization.

**KEYWORDS**

electron microscopy, myelin precursors, olfactory cortex, oligodendrocytes, immunohistochemistry, RRID: AB_10141047, RRID: AB_2236897, RRID: AB_11213678, RRID: AB_2057371, RRID: AB_2140491

## 1 | INTRODUCTION

The onset of myelination is a significant milestone in the development of neural circuits in humans (Jakovcevski et al., 2009) and rodents (Downes & Mullins, 2014) as myelin provides trophic and structural support for axons and substantially increases conduction velocity (Aggarwal et al., 2011). Disrupted myelinogenesis, occurring naturally in developmental forms of leukodystrophy, results in a broad array of symptoms similar to those observed in demyelinating disorders such as multiple sclerosis (Medina, 1993; Padiath et al., 2006). The timing of myelination differs between functional systems and brain regions (Foran & Petersen, 1992; Sampaio & Truwit, 2001) and continues well into postnatal life (Baumann & Pham-Dinh, 2011; Gottlieb et al., 1977; Watson et al., 2006).

The olfactory system is crucially important for mammals at birth as odors provide information essential for pups to locate sustenance and recognize caregivers (Logan et al., 2012). Two large myelinated tracts exclusively carry olfactory information: the lateral olfactory tract (LOT) and anterior limb of the anterior commissure (AC). These two tracts are functionally and geographically distinct (Figure 1). The LOT, found on the ventrolateral surface of the telencephalon, consists of axons carrying sensory information from the olfactory bulb (OB) to olfactory cortices. Axons from OB mitral cells project into the LOT very early during development, beginning around embryonic day (E)13 in mice and continuing until E16. By 2 weeks after birth, collateral projections are well established (Blanchart et al., 2006; Brunjes et al., 2014; Walz et al., 2006).

Two regions of the olfactory cortex, the anterior olfactory nucleus (AON) and anterior piriform cortex, project across the midline via the AC to homologous structures on the contralateral side (Brunjes, 2013; Haberly & Price, 1978). The AC is well separated from olfactory

  

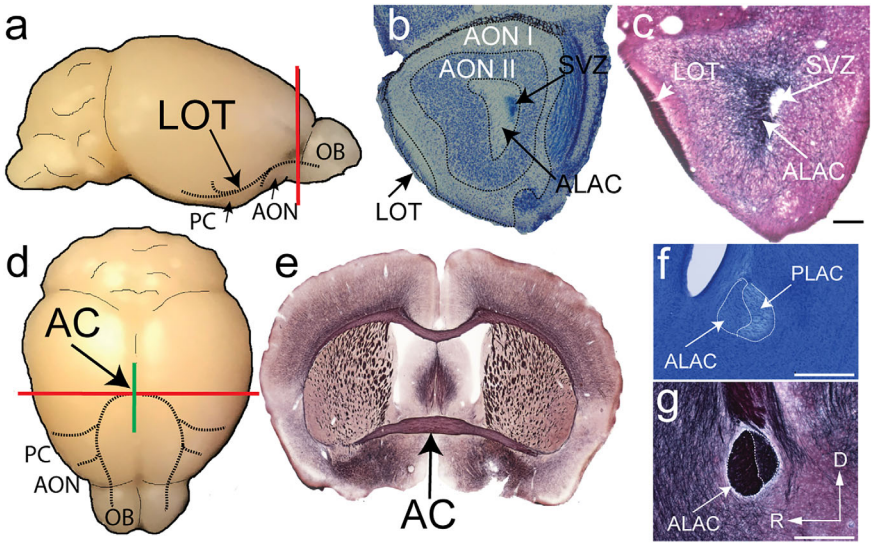


**FIGURE 1** General organization of the LOT and AC. (a) Lateral view of the mouse brain. The LOT (dotted line) originates in the OB and projects ipsilaterally to the AON and piriform cortex (PC). Solid red line indicates the approximate level of coronal (b) Nissl- and (c) myelin-stained sections. Myelin stained with Black Gold (Schmued, 1990). (b) The LOT (arrowhead), on the ventrolateral surface of the olfactory peduncle, is adjacent to the AON pars lateralis. The AON is comprised of two zones, the outer plexiform (AON I) and an inner cellular (AON II) layer. The anterior (olfactory) limb of the AC (ALAC, arrow) courses lateral to the rostral migratory stream (subventricular zone: SVZ) in the center of the olfactory peduncle. (c) Myelin-stained section through similar region demonstrating the location of the LOT and AC. (d) Dorsal view of the mouse brain. The AC (dotted line) contains axons arising in the AON and PC that innervate the contralateral PC, AON, and OB. Solid red line indicates the approximate level of coronal section in (e) and the green, midsagittal line depicts the plane of section in panels (f) and (g). (e) Myelin-stained coronal section at the level where the AC crosses the midline. (f and g) Sagittal sections taken near the midline demonstrate a clear difference between the anterior (olfactory, ALAC) and posterior (PLAC) limbs of the AC in both cell body density (f, Nissl stain) and extent of myelination (g, myelin stain). D = dorsal; R = rostral

processing regions. It is about 4 mm caudal to the OB in mice, and runs deep in the olfactory cortex, well away from the LOT (Figure 1d). While the AC is composed of three divisions, only the anterior limb carries olfactory information (Brunjes, 2013). There has been little work on the postnatal development of the anterior limb of the AC (Sturrock, 1976) though our previous results indicate that a rapid increase in myelin basic protein (MBP) expression occurs from postnatal day (P)11-P14 (Brunjes et al., 2014).

In this study, the onset and progression of myelination in the LOT and AC were examined in several ways. First, oligodendrocyte maturation was tracked based on the expression of several molecular indices including an early precursor marker (platelet-derived growth factor receptor α, PDGF; Calver et al., 1998; Fruttiger et al., 1999; Pringle et al., 1992), a later precursor marker (neural-glial antigen 2, NG2; Nishiyama et al., 2009, 1996; Rivers et al., 2008), a marker for mature oligodendrocytes (CC1; Bhat et al., 1996; Ness et al., 2005), a marker for compact myelin sheaths (MBP; Asou et al., 1995; Shiota et al., 1989), and one oligodendrocyte transcription factor expressed at all stages of development (Olig2; Takebayashi et al., 2002). Second, electron microscopy (EM) was used to quantify developmental changes in myelin sheath thickness and myelinated axon caliber in each tract as well as the numbers and percentages of myelinated axons. Functional differences in the composition of the two tracts were tested by measuring their conduction velocities. Finally, the effects of early sensory deprivation on LOT and AC myelination were assessed. Substantial evidence indicates that experience plays a critical role in developing and maintaining proper central nervous system (CNS) myelination. For instance, early social isolation results in oligodendrocytes with shorter myelinating processes, fewer branch points and fewer internodes in the prefrontal cortex as well as impaired performance on social interaction and working memory tasks (Makinodan et al., 2012). Light deprivation alters myelin formation as well as conduction velocity within the optic nerve (Etxeberria et al., 2010). Functional deprivation is easily accomplished in the olfactory system by surgically closing one naris, reducing airflow and odorant availability in one half of the nasal cavity (Brunjes, 1994; Coppola, 2012). Naris occlusion has been demonstrated to cause many changes in the OB including a 25% reduction in volume by P30. Deprivation of primary sensory information might not have the same effect on the myelination of the LOT and AC due to their different roles in olfactory processing. To test this hypothesis, a separate group of animals underwent unilateral naris occlusion on P1 were reared until P30 and were analyzed for differences in oligodendrocyte maturity and extent of myelination.

## 2 | MATERIALS AND METHODS

### 2.1 | Animals

Male and female C57BL/6J mice (Jackson Labs; Bar Harbor, ME) were housed in standard polypropylene cages with food (8604, Harlan, Frederick, MD) and water ad libitum in a temperature-controlled room on a 12:12 light:dark cycle. Data were collected from three to eight pups for

**TABLE 1** Antibodies

| Antigen | Immunogen | Manufacturer | RRID | Cat./lot number | Species | Dilution |
|---|---|---|---|---|---|---|
| Olig2 | Recombinant mouse Olig2 | Millipore (Temecula, CA) | AB_10141047 | AB9610 2728398 | Rabbit polyclonal | 1/500 |
| PDGF-Rα | Mouse myeloma cell line NS0-derived recombinant mouse PDGF-Rα | R&D Systems (Minneapolis, MN) | AB_2236897 | AF1062 HMQ0215111 | Goat polyclonal | 1/200 |
| NG2 | NG2 chondroitin sulfate proteoglycan from rat | Millipore (Temecula, CA) | AB_11213678 | AB5320 2517782 | Rabbit polyclonal | 1/200 |
| CC1/APC | Recombinant protein consisting of amino acids 1–226 of APC | Millipore (Temecula, CA) | AB_2057371 | OP80 D00172565 | Mouse monoclonal | 1/500 |
| MBP | Human myelin basic protein | Millipore (Temecula, CA) | AB_2140491 | NE1019 D00174372 | Mouse monoclonal | 1/500 |

each measure on P7, 9, 10, 11, 13, 15, 17, 20, 25, and 30 (the day of birth = P0). A separate group of animals underwent unilateral naris occlusion, accomplished by anesthetizing P1 pups via hypothermia and briefly applying a cautery to the right external naris, and then rearing the pups to P30 (Coppola, 2012). Preliminary observations indicated no differences between male and female pups at these early ages; as a result, each treatment group consisted of both sexes. Finally, conduction velocities were measured in 3-month-old adult female mice. All procedures were performed according to National Institutes of Health guidelines and protocols approved by the University of Virginia IACUC.

## 2.2 | Analysis of oligodendrocyte maturation

Mice were deeply anesthetized with sodium pentobarbital (Euthasol; 0.39 mg drug/g body weight; 150 mg/kg; APP Pharmaceuticals; Schaumburg, IL) and perfused intracardially with 0.01 M phosphate buffered saline (PBS; pH 7.4) followed by 4% buffered formaldehyde. Brains were post-fixed for at least 2 hr. Sixty micrometer coronal vibratome sections were rinsed four times for 5 min in PBS, and then incubated in 0.01 M citrate buffer (pH 8.5) at 80°C for 25 min (Jiao et al., 1999). Tissue was cooled to room temperature, washed twice in PBS for 3 min, and permeabilized in 0.03% Triton in PBS (TW). Sections were then placed into a blocking solution (0.5% normal donkey serum in TW; Jackson ImmunoResearch, West Grove, PA) for 1 hr, followed by overnight incubation in primary antibody (Table 1) at 4°C.

Sections were then rinsed four times in PBS and placed in a secondary antibody solution (1/250–1/500 in TW: Jackson ImmunoResearch, donkey anti-rabbit: Catalog number, 711-165-152 or 711-545-152; donkey anti-goat: 705-165-147 or 705-545-147; donkey anti-mouse: 715-485-150 or 715-545-151) for 2 hr. Tissue went through a final 4 × 5 min PBS rinse before being mounted on slides with SlowFade mounting media (Invitrogen: S36937).

## 2.3 | Antibody characterization

Cells within the oligodendrocyte lineage were identified using a rabbit polyclonal antibody against the protein encoded by the Olig2 gene, which is specific to the basic helix-loop-helix transcription factor expressed in oligodendrocytes (Millipore, Cat# AB9610). This antibody recognizes the ~32 kDa Olig2 protein as shown with western blotting on mouse brain lysate (manufacturer's product insert, Table 1) and has been verified for use in labeling both immature as well as mature oligodendrocytes (Mateo et al., 2015; Wahl et al., 2014). Specificity of staining to oligodendrocytes in our samples was confirmed by an absence of labeling in neurons and dense labeling in white matter tracts.

Oligodendrocyte precursors were identified using a rabbit polyclonal antibody against the NG2 integral membrane chondroitin sulfate proteoglycan (Millipore, Cat# AB5320) and a goat polyclonal antibody against the PDGF receptor α (R&D Systems, Cat# AF1062). Specificity of the antibody to the ~320 kDa NG2 protein has been confirmed by western blot (Shearer et al., 2003). The NG2 protein is found on the surface of a group of cells which demonstrate properties of O-2A (oligodendrocyte-type 2 astrocyte) progenitor cells. The NG2 proteoglycan has been found on nonoligodendroglial cells such as pericytes (Stanton et al., 2015) and tumor cells (Al-Mayhani et al., 2011) but within white matter tracts is largely restricted the surface of oligodendroglia prior to terminal differentiation (Dawson et al., 2003). While NG2 is not expressed in all oligodendrocyte progenitor cells, NG2 immunopositive cells represent a significant proportion of precursor cells within the oligodendrocyte lineage (Nishiyama et al., 1996). Specificity to the 160–200 kDa PDGFRa protein has been confirmed through western blots (manufacturer's product insert, Table 1) and a lack of staining in conditional PDGFRa knockout mice (Matoba et al., 2017). PDGFRa is found on many types of proliferating cells, including immature oligodendrocytes (Bergsten et al., 2001; Gilbertson et al., 2001).

Mature oligodendrocytes were identified using a mouse monoclonal antibody against the tumor suppressor adenomatous polyposis coli (APC; Millipore, Cat# OP80). Specificity to the ~321 kDa APC protein has been confirmed via western blots (Smith et al., 1993). APC is a genetic clone of CC1, which has been shown to be specific to oligodendrocytes in the rodent CNS (Bhat et al., 1996). Myelin sheaths were identified using a mouse monoclonal antibody against the ~21 kDa form of MBP (Millipore, Cat# NE1019). Specificity to myelin sheaths has been confirmed in both developing and mature myelin sheaths through co-expression with proteolipid protein, a known component of myelin sheaths (Grishchuk et al., 2015). Labeling in our samples was consistent with known patterns of myelination in the CNS.

## 2.4 | Imaging and analysis

To facilitate comparisons across ages and subjects, only sections from standardized locations were used to gather data. For the LOT, sections were chosen in which the AON forms a complete ring around the subventricular zone (Figure 1b,c). For the AC, sections were chosen at the point where the AC crosses the midline (Figure 1e). Analysis of the AC sections was restricted to the area ~1 mm to each side of the midline in order to assure that only the anterior limb of the AC was sampled. Images were taken with a 20× objective using a Nikon 80i confocal microscope (Nikon Instruments, Inc., Melville, NY). Three optical sections separated by 3 μm were imaged and collapsed. Image montages were constructed and minimally adjusted for brightness and contrast with Adobe Photoshop (San Jose, CA). Within the area of analysis, total numbers of labeled cell bodies were counted. A cell body was counted if part of a somatic profile could be discerned. Because this counting method might overestimate the density of larger cells and because the markers we used are known to target different stages in the lineage of one population of cells, we were careful to confirm that there were no differences in the size of the labeled figures that might bias cell counts. Mean cell soma profile diameter was calculated using ImageJ (Rasband, 1997) for 50 cells for each marker (Guillery & Herrup, 1997). No differences were found between Olig2 ($M = 7.86 \pm SD = 1.16$ μm), PDGF ($8.60 \pm 2.03$ μm), NG2 ($8.11 \pm 1.70$ μm) and CC1 ($8.75 \pm 2.22$ μm; $F = 2.62$, $p = .06$), indicating that there was an equal probability of encountering any labeled cell type in a given sample. These findings indicate that the different cell populations do not differ significantly in size and therefore no sampling correction was applied. They further suggest that as oligodendrocytes progress through early stages, relatively little change occurs in cell body size. Cell density was calculated for Olig2, PDGF, NG2, and CC1 by dividing the number of labeled cells by the measured area of the LOT or AC. For MBP, which does not label somata, images were converted to 8-bit black and white images, Image J's white default thresholding setting was applied, and the area fraction measurement (A/A: proportion of labeled to total pixels) obtained to estimate developmental changes in labeling. Means and standard deviations were calculated and one-way analyses of variance with Bonferroni's multiple comparison post hoc tests were used to determine differences between groups.

## 2.5 | Analysis of myelin development

A separate group of animals (three animals/age group: P7, 9, 11, 13, 15, 17, 20, 25, 30) was perfused with a solution containing 2% paraformaldehyde and 2% glutaraldehyde. Their brains were removed and post-fixed for at least 2 hr and then sectioned in the coronal plane at 60 μm with a vibratome and the specimens prepared for EM. Tissue was rinsed with 0.1% phosphate buffer (PB) and postfixed with $OsO_4$ for 1 hr. Following post-fixing, tissue was sequentially dehydrated, counterstained with 4% uranyl acetate in 70% ethanol for at least 1 hr and embedded in EPON resin. Tissue was then sectioned using an ultramicrotome (Leica UC7). Images were taken at either 2,500× or 6,000× magnification with a JEOL 1010 transmission electron microscope. Axons were considered to be promyelinated if an oligodendrocytic process had begun wrapping the profile and myelinated if multiple (>1.5) complete wraps of myelin sheath could be observed. Counts of unmyelinated, promyelinated, and myelinated axons per unit area were made and samples of more than 1,000 axons from at least two animals were used to estimate the percentage of axons myelinated, promyelinated, or unmyelinated at P11, 13, 15, 17, 20, 25, and 30. Myelin thickness was measured as the distance between the innermost and outermost point of compacted segments (Figure 6b). Axon caliber was estimated by calculating the diameter of a circle with the same circumference as the perimeter of myelinated axons. For naris occlusion studies, g-ratios (Chomiak & Hu, 2009; Rushton, 1951) were calculated by dividing the axon caliber by the diameter of the combined axon and myelin sheath. ImageJ was used for all measurements. Means and standard deviations were calculated for each animal on each measure and non-parametric statistics (Mann–Whitney *U* and Kruskal–Wallis *H* tests) were used to determine differences between groups.

## 2.6 | Measurements of conduction velocity

Three-month-old female mice were sedated with a 0.32 mg/kg, i.m. injection of medetomidine hydrochloride (Domitor, Pfizer Animal Health), anesthetized with 40 mg/kg, i.m., ketamine hydrochloride (Ketaset, Fort Dodge Animal Health) and placed into a stereotaxic instrument. For studies of the AC, a bipolar stimulating electrode (WE3CEA3, Microprobes, Gaithersburg, MD) and a tungsten monopolar recording electrode (30020, FHC, Bowdoin ME; ~0.5MΩ) were placed on opposite sides of the brain ~2.0 mm rostral to bregma, 1.5 mm lateral to the midline and 3.4 mm ventral to surface of the brain. For studies of the LOT stimulating electrodes were placed approximately 2.0 mm rostral to bregma, 3.4 lateral of the midline and 2.0 mm ventral to the surface of the brain while recording electrodes were located 2.0 mm caudal to bregma, 3.4 lateral of the midline and 3.4 mm ventral to the surface of the brain. Rhythmic electrical stimuli were administered in at least three positions: when recording electrodes were ~0.2–0.3 mm superficial to the target, at the target site, and ~0.2 mm deeper than the target site. After data were collected the position of the stimulating electrode was varied either 0.2 mm deeper or superficially and new recordings then made from the deep, target and superficial sites again. At each position trains of 10–15 pulses (0.2 ms positive) were administered at 10 intensities ranging from 0.01–1 mV. Recordings of evoked potentials were made with Chart software (ADInstruments). Electrode placement was verified histologically in cases where stimulus-evoked changes were confined to the target location. Mice were perfused as described above and serial 60 μm vibratome sections collected and Nissl-stained. Section thickness was verified in control tissue by staining all cells with a fluorescent marker (Sytox, S7020, Molecular Probes) and the top and bottom borders of the section located with a confocal microscope. The averages of these measurements were nearly identical (<2%) with the nominal 60 μm. Estimates of the distance between stimulating and recording electrodes were made from 3D reconstructions of the brains with Neurolucida, (MBF Biosciences, Williston, VT). The time between stimulation offset

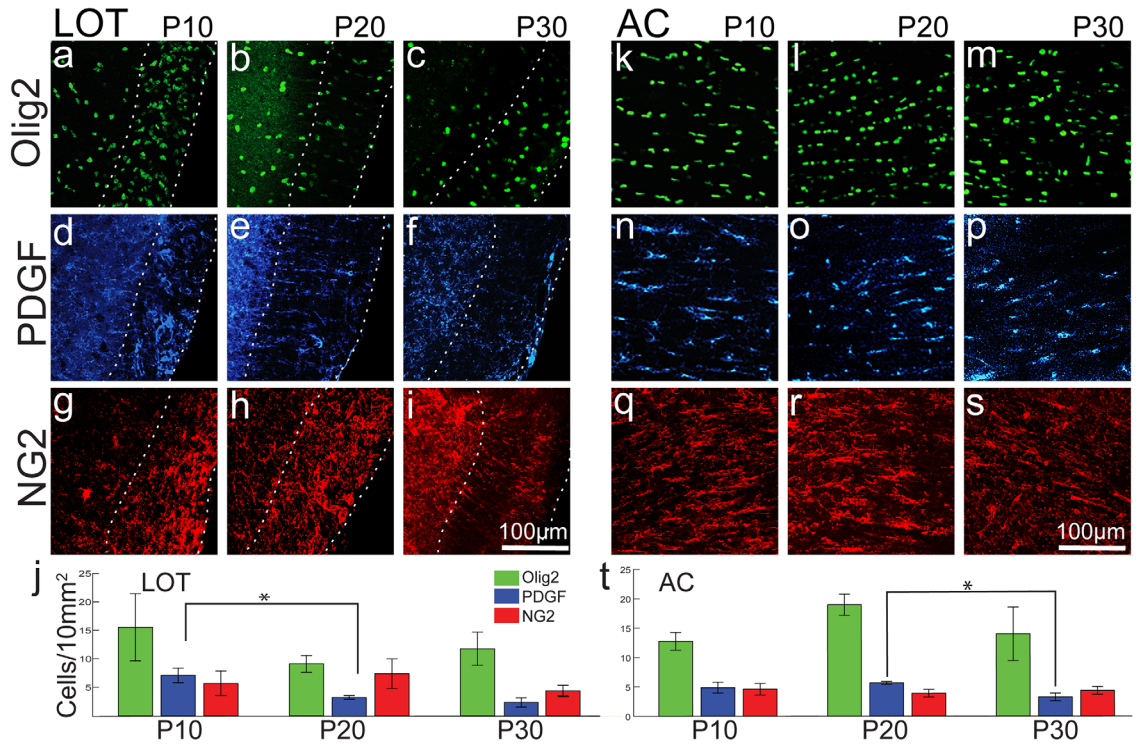


**FIGURE 2** Early oligodendrocyte maturation in the developing LOT and AC, including representative sections immunostained for Olig2, PDGF, or NG2 at P10, 20, and 30. Dotted lines indicate tract boundaries. (j and t) Quantification of cell density of Olig2 (green), PDGF (blue), and NG2 (red) in the LOT and AC. Olig2 labeling (a marker for all cells in the oligodendroglial lineage) did not change over time in either tract (a–c, k–m). Developmental changes in PDGF + cell density were observed between the LOT and AC. A significant decrease in PDGF labeling was observed in the LOT between P10 and P20 (j) and in the AC between P20 and P30 (t). NG2 labeling remained consistent over time in both tracts. Error bars represent standard deviation. $^*p < .05$

and the peak of the evoked potential measured in the recording electrodes was measured offline with Chart software (ADInstruments).

## 3 | RESULTS

### 3.1 | Survey of postnatal development: light microscopy

To provide a general overview of myelination, three ages were chosen for examination: P10 (an immature stage before ear or eye opening), P20 (near weaning), and P30 (when OB growth has reached asymptote; Hinds & Hinds, 1976; Rosselli-Austin & Altman, 1979). All measurements were made at the standardized locations described above (Figure 1).

#### 3.1.1 | Lateral olfactory tract

As a first step, the total density of all cells in the oligodendrocyte lineage was determined using the pan-oligodendroglial marker Olig2. In the LOT, Olig2+ cell density was higher at P10 (Mean = 15.55 ± 5.91 cells/10 mm$^2$) than at P20 ($M = 9.11 \pm 1.47$ cells/10 mm$^2$) or P30 ($M = 11.77 \pm 2.92$ cells/10 mm$^2$; Figure 2a–c,s), although no statistically significant trends were found. To determine whether the higher density of Olig2+ cells seen in early ages could be attributed to a high precursor population, two glial precursor cell markers that are co-expressed in early progenitor cells (Nishiyama et al., 2009) were used. While both PDGF and NG2 label a significant proportion of oligodendrocyte progenitor cells, neither antigen alone labels the entire population (Nishiyama et al., 2009, 2002). A developmental decrease in PDGF+ cell density was observed during the study period, with most of the change occurring between P10 ($M = 7.09 \pm 1.29$ cells/10 mm$^2$) and P20 ($M = 3.93 \pm 0.32$ cells/10 mm$^2$; $t = 4.374$, $p < .05$, Figure 2g–i,s). A further decrease occurred by P30 ($M = 2.41 \pm 0.77$ cells/10 mm$^2$). NG2 showed a different developmental pattern, with little change over time ($F = 1.636$, n.s.; Figure 2m–o). NG2+ precursor cell density at P10 ($M = 5.67 \pm 2.19$ cells/10 mm$^2$) was statistically similar to that seen at both P20 ($M = 7.38 \pm 2.60$ cells/10 mm$^2$) and P30 ($M = 4.38 \pm 0.97$ cells/10 mm$^2$; Figure 2s). The large decrease in PDGF staining between P10 and P20 suggested that during this period a substantial proportion of oligodendrocytes in the LOT reach maturity.

To confirm the developmental changes suggested by precursor labeling, terminally differentiated oligodendrocyte density was determined by the expression of CC1, and the maturation of myelinating sheaths was assessed by the expression of MBP. CC1 staining significantly changed with age ($F = 5.24$, $p < .05$) with a substantial increase occurring between P10 ($M = 4.01 \pm 1.06$ cells/10 mm$^2$) and P20 ($M = 12.75 \pm 3.11$ cells/10 mm$^2$; $t = 2.84$, $p < .05$) and a 65% decrease by P30 ($M = 8.32 \pm 4.69$ cells/10 mm$^2$; Figure 3a–g). At P20 and P30 CC1+ cells exhibited a similar density as Olig2+ cells, indicating that

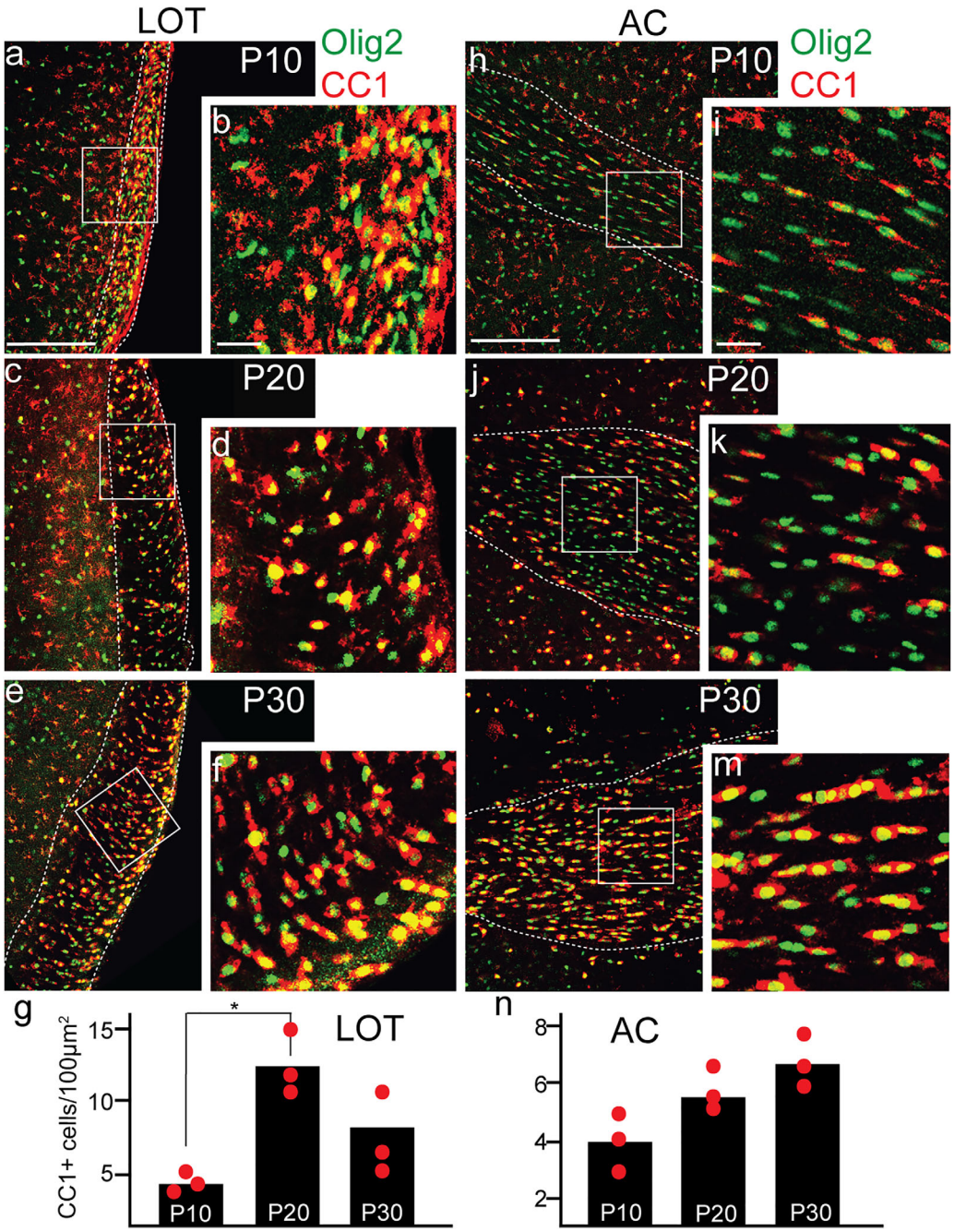


**FIGURE 3** Later oligodendrocyte maturation in the developing LOT and AC. Representative LOT (a–f) and AC (h–m) sections immunostained for Olig2 (green) and CC1 (a marker for mature oligodendrocytes; red) at P10, 20, and 30. Dotted white boxes represent area enlarged in inset panels at right. Note the increase in colabeling (yellow) over time in both the LOT and AC. Scale bar = 100 μm. Inset scale bar = 50 μm. (g,n) Quantification of CC1 staining confirmed that between P10 and 20 large increases in CC1+ cell density occurred in the LOT while in the AC a more slight, steady increase was observed. Circles represent mean recorded density for each animal and bars represent average density across three animals. $^{*}p < .05$

by that time most Olig2+ cells in the LOT are mature oligodendrocytes (Figure 3d,f). Co-labeling of Olig2 and CC1 confirmed that by P20 most Olig2+ cells are also CC1+. Indeed, substantial myelination was already exhibited by P10 in the LOT as evidenced by the density of MBP staining (A/A = 33.85 ± 5.33; Figure 4a). At this time, the AON showed no signs of myelination (Brunjes et al., 2014). The amount of MBP labeling in the LOT increased across the period observed ($F = 47.78$, $p < .001$). Between P10 and P20 MBP labeling almost doubled (A/A = 64.66 ± 7.6; $t = 6.90$, $p < .01$) and slightly rose by P30 (A/A = 76.04 ± 1.73; $t = 2.55$, n.s.; Figure 4a–d).

### 3.1.2 | Anterior commissure

At P10 both the LOT and AC exhibited similar Olig2+ cell density (AC: $M = 12.78 \pm 1.51$ cells/10 mm$^2$). Density peaked at P20 ($M = 18.96 \pm 1.82$ cells/10 mm$^2$) and slightly decreased by P30 ($M = 14.01 \pm 4.55$ cells/10 mm$^2$; Figure 2d–f,t). Similar to the LOT, PDGF+ precursor cell

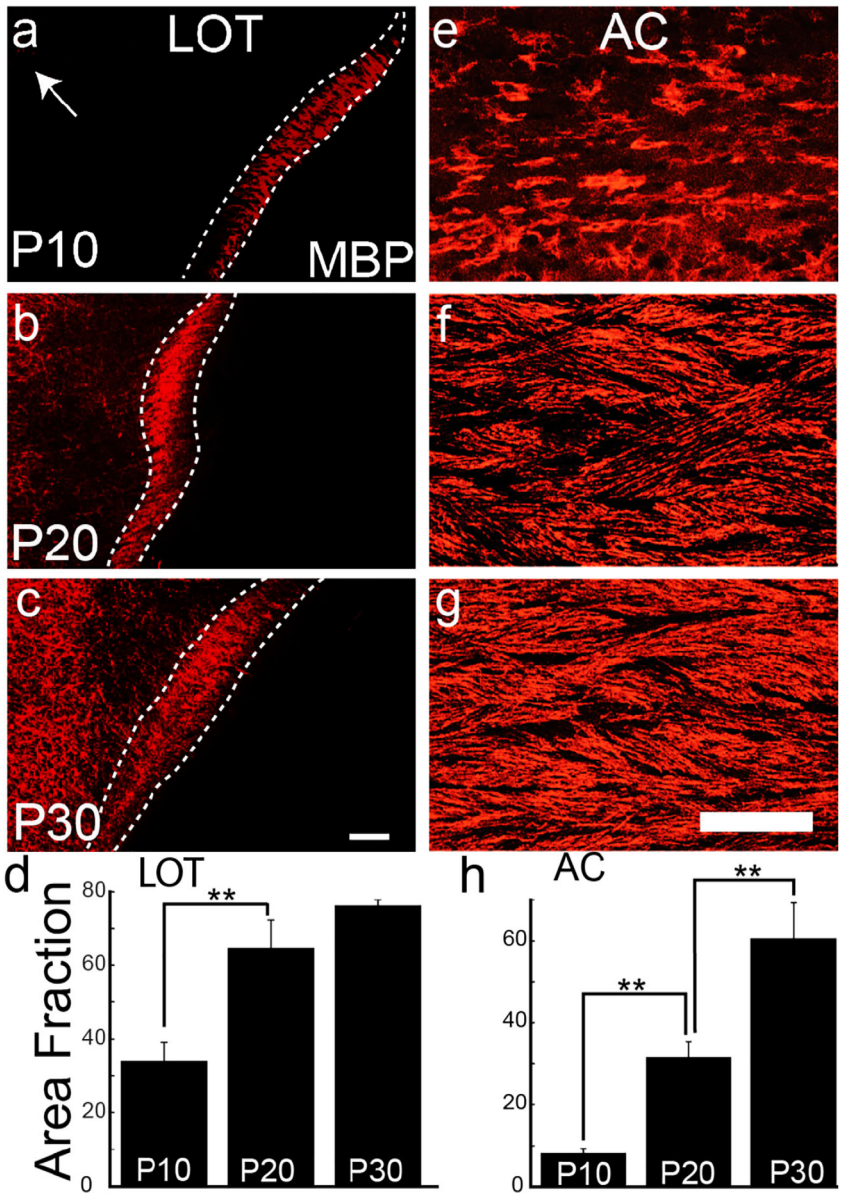


**FIGURE 4** Development of myelin sheaths in the LOT and AC. Representative LOT (a–c) and AC (e–g) sections immunostained for MBP, a marker of myelin sheaths, at P10, 20, and 30. Note the high-staining density in the LOT as early as P10 (a), a time when very little myelin can be seen in the anterior limb of the AC (arrow) as it extends through the AON or in the AC as it crosses the midline (e). A rapid increase in MBP labeling occurred in the LOT between P10 (a) and 20 (b), confirmed by quantification of the area fraction (proportion of labeled to total pixels. (d) Note the difference in the timing of myelination between the LOT and the adjacent AON pars lateralis. While little myelin staining is present in the AON at P10, a large increase occurs between P20 and 30 (b,c). Significant increases in MBP labeling were observed in the AC between P10 and 20 as well as between P20 and 30 (e–h). Scale bars = 100 μm. Error bars represent standard deviation. $^{**}p < .01$

populations in the AC decreased over time ($F = 10.03$, $p < .05$), but the change occurred later. No difference was observed between P10 ($M = 4.88 \pm 0.93$ cells/10 mm$^2$) and P20 ($M = 5.66 \pm 0.24$ cells/10 mm$^2$), but a significant decrease occurred by P30 ($M = 3.25 \pm 0.66$ cells/10 mm$^2$; $t = 4.39$, $p < .05$; Figure 2j–l,t). NG2 labeling followed a different pattern than PDGF, with no significant changes over time ($F = 0.651$, n.s.; Figure 2p–r,t). At P10, the density of NG2+ cells ($M = 4.61 \pm 0.98$) was statistically similar to the values recorded at P20 ($3.89 \pm 0.65$ cells/10 mm$^2$) and P30 ($M = 4.35 \pm 0.65$ cells/10 mm$^2$). At P10, the AC showed little evidence of myelination, with low CC1 staining ($M = 4.03 \pm 1.14$ cells/10 mm$^2$; Figure 3h–i) and few nascent MBP+ sheaths present (A/A= $8.01 \pm 1.32$; Figure 4e). CC1 staining increased between P10 ($M = 4.03 \pm 1.14$ cells/10 mm$^2$) and P20 ($M = 5.78 \pm 0.87$ cells/10 mm$^2$) and continued to rise to P30 ($M = 6.56 \pm 1.02$ cells/10 mm$^2$; Figure 3h–n). Between P20 and P30, a large increase in the number of cells co-expressing Olig2 and CC1 was observed (Figure 3j–m). MBP staining rapidly increased across time ($F = 66.07$, $p < .0001$). A large (292%) increase in MBP labeling was

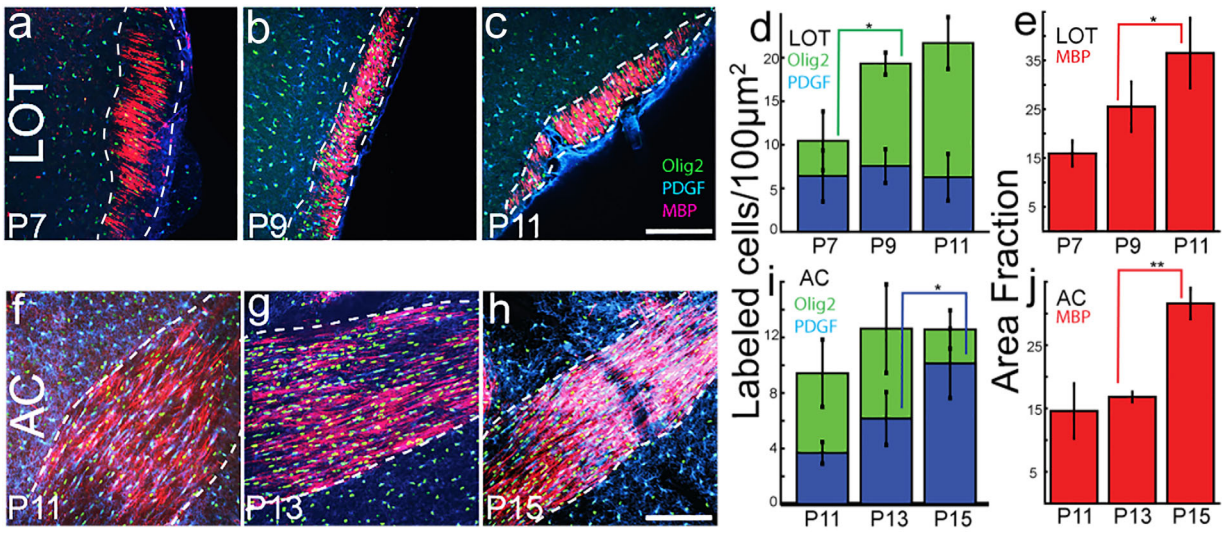


**FIGURE 5** Comparison of the period of rapid myelination in the LOT and AC. Tissue was immunostained for Olig2 (green), PDGF (blue), and MBP (red). (a–c) Representative LOT sections from mice aged P7, 9, and 11; (f–h) depict AC sections from P11, 13, and 15. Scale bar = 100 μm. (d,e,i,j) Quantification of developmental changes in immunostaining for each of the antigens (Olig2, green; PDGF, blue; and MBP, red). Note that as early as P7 MBP labeling is present in the LOT (a,e) and that the presence of PDGF+ precursor cells remained high in the AC as late as P15 (h,i), confirming an earlier developmental trajectory of the LOT. Error bars represent standard deviation. $^{*}p < .05$, $^{**}p < .01$

observed between P10 and P20 (A/A = 31.39 ± 4.05; $t = 5.11$, $p < .01$) and an additional 93% increase occurred between P20 and P30 (A/A = 60.51 ± 8.72; $t = 6.36$, $p < .01$; Figure 4e–h).

## 3.2 | Period of rapid myelination: Light microscopy

The data above indicate that the LOT and AC have different times of rapid myelination. Therefore, a second study more closely defined the time course of these changes. Three early ages (P7, 9, and 11) were chosen for a closer examination of the LOT because mature myelinating cells were already present by P10. Later ages (P11, 13, and 15) were chosen for AC analyses based on data presented above as well as previously reported results (Brunjes et al., 2014). Tissue was stained for expression of Olig2, PDGF, and MBP as these markers showed the largest changes across P10–30 and allow for distinguishing between all oligodendrocytes (Olig2+), oligodendrocyte precursor cells (PDGF+), and mature myelin sheaths (MBP+).

### 3.2.1 | Lateral olfactory tract

The total density of Olig2+ cells in the LOT significantly changed over the interval examined ($F = 14.29$, $p < .01$), almost doubling between P7 ($M = 10.44 \pm 3.39$ cells/10 mm$^2$) and P9 (19.31 ± 1.28 cells/10 mm$^2$; $t = 4.01$, $p < .05$) and leveling off at P11 ($M = 21.67 \pm 2.99$ cells/10 mm$^2$; Figure 5a–d). During this period, the density of oligodendrocytes remained much higher than the value recorded at P30, likely a result of large increases in area of the LOT after P11. PDGF+ cell density at all ages was similar to that observed at P10 (P7 $M = 6.39 \pm 2.93$ cells/10 mm$^2$, P9 $M = 7.53 \pm 1.93$ cells/10 mm$^2$, P11 $M = 6.25 \pm 2.67$ cells/10 mm$^2$; $F = 0.23$, n.s. Figure 5a–d). As early as P7 MBP labeling was detected (A/A = 15.94 ± 2.43). Staining increased significantly during the period ($F = 11.65$, $p < .01$), with the largest increase observed between P9 (A/A = 25.53 ± 4.91) and P11 (A/A = 36.51 ± 6.98; $t = 3.39$, $p < .05$; Figure 5a–c,e). At P11m MBP staining was approximately half the value recorded at P20, indicating that myelination continues to occur throughout the preweanling period.

### 3.2.2 | Anterior commissure

A different pattern was observed during the onset of rapid myelination in the AC (Figure 5f–j). Unlike in the LOT, Olig2+ oligodendrocyte density did not change over the period observed (P11 $M = 9.42 \pm 2.42$ cells/10 mm$^2$, P13 $M = 12.63 \pm 3.18$ cells/10 mm$^2$, P15 $M = 12.58 \pm 1.38$ cells/10 mm$^2$; $F = 1.7$, n.s.; Figure 5i) and remained slightly lower than the density observed at P30. However, a large increase in precursor cell density was observed across the period examined. PDGF staining increased steadily from P11 to P15 with a 60% increase observed between P11 ($M = 3.69 \pm 0.77$ cells/10 mm$^2$) and P13 ($M = 6.16 \pm 1.90$ cells/10 mm$^2$) and an additional 61% increase by P15 ($M = 10.13 \pm 2.50$ cells/10 mm$^2$; $F = 9.09$, $p < .05$; Figure 5i). Myelination as measured by MBP staining also increased over time. Labeling stayed stable between P11 (A/A = 14.61 ± 4.20) and P13 (A/A = 16.83 ± 0.65; $t = 0.97$, n.s.) but significantly increased by P15 (A/A = 31.59 ± 2.31; $t = 6.47$, $p < .01$; Figure 5f–h,j). Once again, at all ages examined MBP staining was lower than the corresponding P30 value, indicating that substantial myelination occurs after P15 in the AC.

## 3.3 | Electron microscopy

An analysis of tissue from P5, 7, 9, 11, 13, 15, 17, 20, 25, and 30 pups was made for both tracts. The presence and density of unmyelinated, pro-myelinated, and myelinated axons were quantified to complement the developmental time courses established by immunological markers.

EM analysis also allowed for measurement of axon caliber and thickness of myelin sheaths.

#### 3.3.1 | Lateral olfactory tract

The first indication of myelination in the LOT was the presence of promyelinating oligodendrocytes at P7 (Figure 6a). The density of promyelinated fibers changed over time ($H = 106.25$, $p < .001$), with a significant increase between P9 ($5.29 \pm 1.46$ axons/100 $\mu m^2$) and P11 ($8.71 \pm 1.96$ axons/100 $\mu m^2$; $U = 0$, $p < .05$) and peaked at P13 ($9.62 \pm 2.38$ axons/100 $\mu m^2$). This increase was followed by a steady nonsignificant decline from P15 ($6.89 \pm 1.41$ axons/100 $\mu m^2$) through P30 ($2.99 \pm 0.75$ axons/100 $\mu m^2$; Figure 6k). The first instances of compact myelin sheaths appeared at P9, and, mirroring the results described above, a sharp increase in number of myelinated axons occurred between P9 and 11 ($7.78 \pm 3.29$ to $43.69 \pm 14.55$ myelinated axons/100 $\mu m^2$; $U = 0$, $p < .05$; Figure 6b,c,m). The density of myelinated axons continued to rise between P15 ($52.95 \pm 13.30$ axons/100 $\mu m^2$) and P20 ($63.53 \pm 5.54$ axons/100 $\mu m^2$) before leveling off (P25 = $62.89 \pm 6.43$ axons/100 $\mu m^2$, P30 = $63.00 \pm 17.86$ axons/100 $\mu m^2$; $H = 11.26$, $p < .0001$; Figure 6m). Percentages of myelinated, promyelinated, or unmyelinated axons were also calculated, with results confirming patterns observed with density calculations (Figure 6o). Between P11 and P13, a sharp increase in the percentage of myelinated (P11 = 1.17%, P13 = 33.70%) and pro-myelinated (P11 = 2.24%, P13 = 5.98%) axons occurred. The percentage of myelinated axons in the LOT increased at every subsequent age (P15 = 45.49%, P17 = 53.27%, P20 = 71.10%, P25 = 78.84%, P30 = 84.10%). Average myelinated axon caliber slightly increased with age ($H = 75.25$, $p < .0001$). At P9, average axon diameter was $1.15 \pm 0.36$ μm. A significant increase was observed by P11 ($1.37 \pm 0.21$ μm; $U = 0$, $p < .05$) and caliber steadily increased through P15 ($1.58 \pm 0.18$ μm). A slight subsequent decrease was recorded from P17 ($1.51 \pm 0.03$ μm) to P30 ($1.46 \pm 0.21$ μm; Figure 6l). Mean myelin thickness also increased across time ($H = 95.21$, $p < .0001$) but was restricted to a range of 0.06 μm (P9 $M = 0.08 \pm 0.03$ μm, P30 $M = 0.14 \pm 0.06$ μm; Figure 6n).

#### 3.3.2 | Anterior commissure

Little evidence of myelination was present in the AC at P11, with only $1.92 \pm 0.12$ promyelinated axons/100 $\mu m^2$ on average and only one myelinated axon per ~20 $\mu m^2$ (Figure 6f,k,m). Numbers of promyelinated axons in the AC rose significantly between P13 ($6.89 \pm 1.82$ axons/100 $\mu m^2$) and P20 ($14.31 \pm 2.53$ axons/100 $\mu m^2$; $U = 0$, $p < .05$), followed by a decrease through P25 ($11.53 \pm 0.90$ axons/100 $\mu m^2$) and P30 ($10.26 \pm 3.97$ axons/100 $\mu m^2$; Figure 6k). Mean density of myelinated axons increased by a factor of nearly 200 (from $0.61 \pm 0.26$ to $117.11 \pm 31.27$ axons/100 $\mu m^2$) between P11 and P30 ($H = 51.18$, $p < .0001$), with two sharp increases between P11 and P13 ($10.87 \pm 3.95$ axons/100 $\mu m^2$; $U = 0$, $p < .05$) and between P17 ($25.38 \pm 7.59$ axons/100 $\mu m^2$) and P20 ($87.24 \pm 15.23$ axons/100 $\mu m^2$; $U = 0$, $p < .05$; Figure 6m). At P30, there was substantial variation in different areas of the AC (from 56.60 to 173.62 myelinated fibers/100 $\mu m^2$), although no consistent patterns were found (Brunjes, 2013). Again, calculations of percent myelinated, promyelinated, and unmyelinated confirmed density measures (Figure 6p). At P11 and P13, <1% of axons in the AC were myelinated. Between P15 and P17, a substantial increase in the percentage of axons myelinated occurred (P15 = 2.60%, P17 = 11.37%). Another large increase was observed between P17 and P20 (21.17% myelinated axons). By P30, the percentage of axons myelinated was 23.12% with 3.97% of axons promyelinated. Mean axon caliber of myelinated axons varied widely and did not significantly change with age ($H = 3.5$, $p = .74$; Figure 6l). Axon diameter of myelinated fibers in early ages (P11 = $0.80 \pm 0.02$ μm, P13 = $0.86 \pm 0.04$ μm, P15 = $0.81 \pm 0.05$ μm) was similar to that of later ages (P20 = $0.75 \pm 0.04$ μm, P25 = $0.82 \pm 0.09$ μm, P30 = $0.94 \pm 0.09$ μm). Mean myelin thickness significantly changed over time ($H = 72.22$, $p < .0001$) but was restricted to a range of 0.018 μm (Figure 6n). The maximum myelin thickness value was recorded at P15 ($0.084 \pm 0.04$ μm) and the minimum recorded at P20 ($0.066 \pm 0.03$ μm).

### 3.4 | Conduction velocity

The observed differences in axon caliber and myelination predict physiological differences between the tracts. These were verified by analysis of conduction velocity in 3-month-old female mice. Signal transfer in the LOT (5.03 m/s, *SEM*: .037) was more than twice as fast as that in the AC (2.07 m/s, *SEM* 0.054 m/s. $t = -21.837$; $p < 4.18E\text{-}09$, Figure 7a,b).

### 3.5 | Unilateral naris occlusion

Given the findings described in the introduction indicating that function affects myelination, it was important to determine if activity also affects development of these two olfactory system tracts. As the bundles carry different aspects of the same information (the LOT carries primary information from the OB to the cortices, while the AC carries processed information between hemispheres), unilateral naris occlusion might differentially affect the two tracts. Deprivation has been shown to have large effects on the developing OB, and to induce changes in the AON and piriform cortex (Brunjes et al., 2014; Coppola, 2012).

#### 3.5.1 | Lateral olfactory tract

The LOT ipsilateral to occlusion in experimental animals was compared to both the contralateral LOT as well as to the LOT of normal controls at P30. To confirm that samples represented similar populations, myelinated axon caliber was compared and found to not vary between groups: mean caliber was consistent in the LOT ipsilateral to occlusion ($M = 1.50 \pm 0.58$ μm), the contralateral LOT ($M = 1.55 \pm 1.01$ μm), and that of control animals (M = $1.46 \pm 0.67$ μm; $H = 5.4$, $p = .07$). In addition, no differences were recorded in the density of myelinated axons between the LOT ipsilateral to occlusion ($61.12 \pm 11.78$ axons/100 $\mu m^2$), contralateral to occlusion ($57.13 \pm 3.83$ axons/100 $\mu m^2$) and controls ($63.00 \pm 17.86$ axons/100 $\mu m^2$; $H = 3.4$, $p = .18$; Figure 7c). Occlusion had two notable effects. First, myelin was significantly thinner in both the LOT ipsilateral ($0.11 \pm 0.06$ μm) and contralateral to occlusion ($0.10 \pm 0.04$

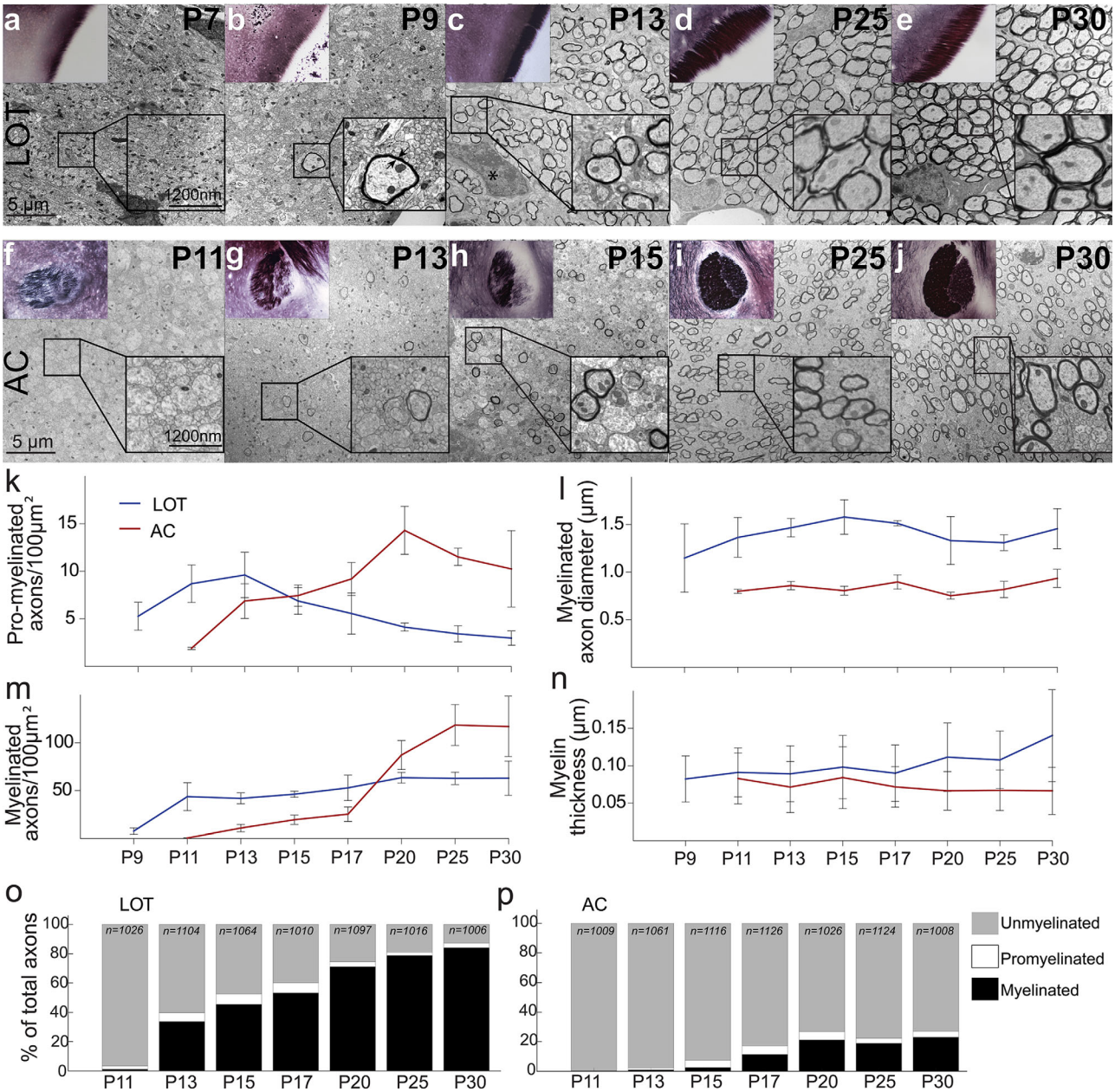


**FIGURE 6** Ultrastructural development of the LOT and AC. Top: Myelin-stained sections (insets) and EM micrographs of the developing LOT (a–e) and AC (f–j). With age the area of the LOT as well as the density of myelin staining increases dramatically, especially between P9 and P13. (a) At P7 no myelinated axons are present, but pre-myelinating oligodendrocyte processes can be seen in between axons (boxed inset). (b) Early myelination was observed at P9, evidenced by myelin wrappings and oligodendrocyte cytoplasm surrounding axons (inset). Myelin thickness was determined by measuring the distance between the inner and outermost point of compacted segments (arrows). (c) Myelinated fibers were more apparent by P13, often clustered nearby glial cells or glial precursor cells (asterisk). (d,e) Average myelinated cell density greatly increased by P25 (d), and continued to increase through P30 (e). Myelin stains demonstrated that with age the AC (f–j, inset) enlarges and the difference between the heavily myelinated anterior limb (left) and the posterior limb (right) becomes more apparent. Very few myelinated fibers were observed in the AC at P11 (f) with only sporadic promyelinated fibers. By P13 (g) the AC has begun myelinating large-caliber fibers. At the same time the LOT contained many myelinated figures (c). A large increase in myelinated fiber density caliber occurs between P13 and P15 (h) that continues through the period observed (i,j). Bottom panels: quantification of ultrastructural development of the LOT and AC. (k) Number of promyelinated axons per 100 $\mu m^2$ in the LOT (blue line) and AC (red line) with age. Promyelinated fibers decreased in density earlier in the LOT (after P13) than in the AC (after P20). (l) Mean axon caliber of myelinated fibers was substantially greater in the LOT than in the AC at every age examined. (m) Myelinated cell counts (number of myelinated axons per 100 $\mu m^2$) increased much earlier in the LOT (between P9 and P11) than the AC (between P17 and 25). (n) Mean myelin thickness was similar throughout the development of both the LOT the AC, but was consistently higher in the LOT compared to the AC. (o,p) Percentages of myelinated (black), promyelinated (white), and unmyelinated (gray) axons in the LOT (o) and AC (p) followed a similar developmental trend to that observed with density measures (k,m)

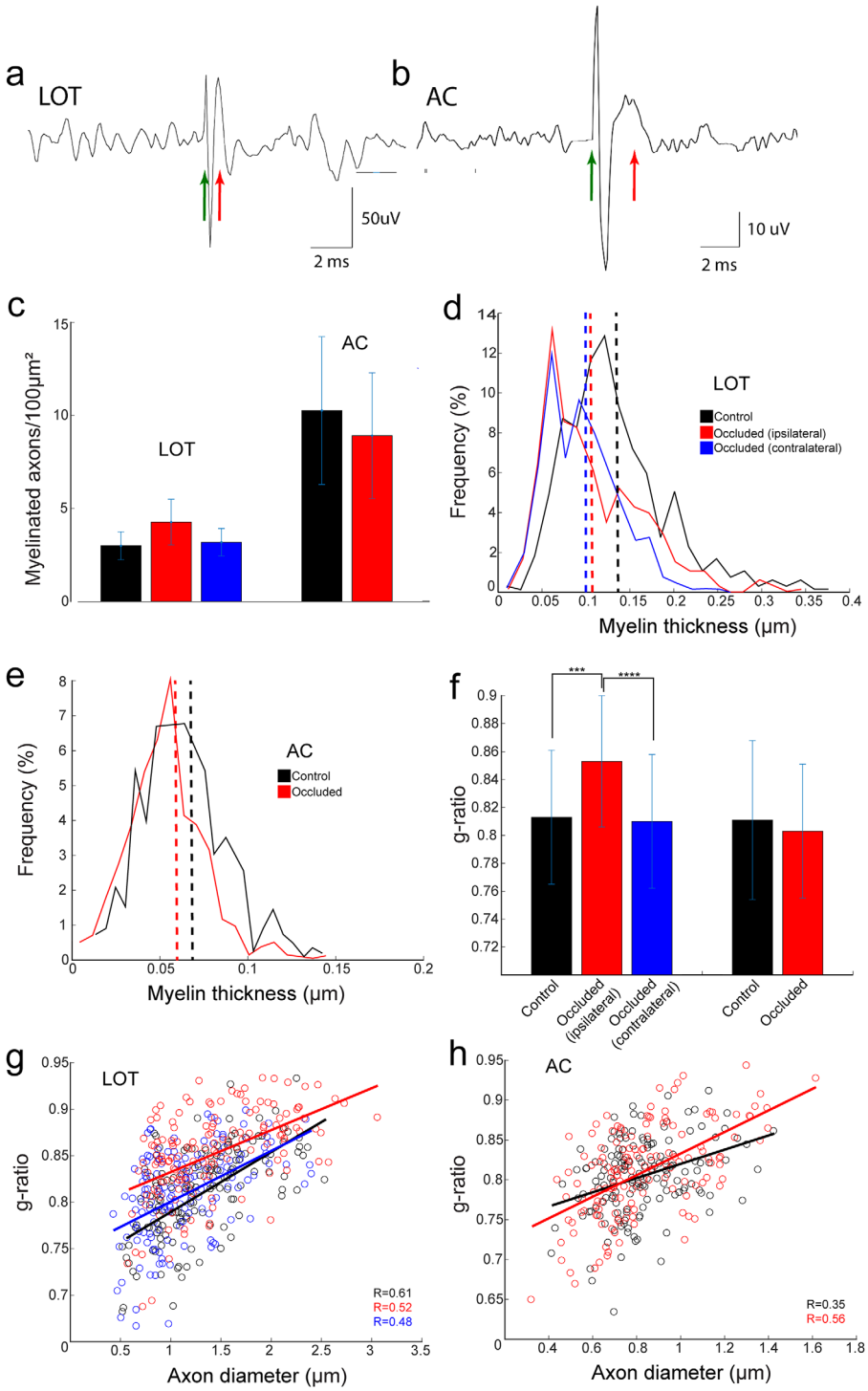


**FIGURE 7** Top: Representative evoked responses in the LOT (a) and AC (b). The interval between time of stimulation (green arrows) and the peak of the evoked responses (red arrows) was estimated and compared. Bottom: Quantification of the effects of unilateral naris occlusion from P1 to P30 on myelination. (c) No differences in the density of myelinated axons was observed between control and experimental animals in the LOT (left) or AC (right). (d) In the LOT, a significant decrease in myelin thickness was observed in experimental animals compared to controls (black) in both the LOT ipsilateral (red) and contralateral (blue) to occlusion. The differences in the average thickness of the myelin sheath (dotted vertical lines) is reflected in frequency histograms: most myelin sheaths fell between 0.05 and 0.1 µm in experimental animals and between 0.1 and 0.15 µm in controls. (e) In the AC, myelin was slightly thinner on average in experimental animals (red) compared to controls and the distributions between control and experimental samples differed significantly. (f–h) To confirm that differences in myelin thickness could not be accounted for by a sampling of thinner axons, g-ratios were calculated and compared. In the LOT, a significant increase in g-ratio (indicating thinner myelin sheaths relative to axon caliber) was observed in the tract ipsilateral to occlusion in experimental animals. However, in the AC, no difference in g-ratio was found, suggesting that the small difference observed in myelin thickness might be due to sampling artifacts. Open circles in (g) and (h) represent individual data points fit with a linear function (solid lines). Error bars represent standard deviation. ***$p < .001$

**TABLE 2** Comparisons between the LOT and AC

| | LOT | AC |
|---|---|---|
| Developmental differences | | |
| Initial tract formation | E13 (Walz et al., 2006) | E16 (Silver et al., 1982) |
| First appearance of myelinated fibers | P7 | P11 |
| Onset of function | Birth (Logan et al., 2012) | P12 (Kucharski & Hall, 1990) |
| Period of rapid myelination | P9–11 | P13–15 |
| Effects of unilateral naris occlusion | Thinner myelin sheaths, fewer pro-myelinated axons | No observed effects |
| Structural differences (>P30 mice) | | |
| Axon caliber (all axons) | 0.768 μm (Brunjes et al., 2011) | 0.553 μm (Brunjes, 2013) |
| Axon caliber (myelinated only) | 1.5 μm | 1 μm |
| Percent myelinated | 84% | 23% |
| Myelin thickness | 0.14 μm | 0.07 μm |
| g-ratio | 0.813 | 0.830 |
| Conduction velocity | 5.03 m/s | 2.07 m/s |

E = embryonic day; P = postnatal day.

μm) compared to age-matched controls (0.14 ± 0.06 μm; $H = 7.2$, $p = .02$; Figure 7d). To confirm that naris occlusion resulted in a thinning of the myelin sheath relative to axon caliber, g-ratios were calculated for 150 axons in occluded and control samples. The difference in myelin thickness was reflected in a significantly larger mean g-ratio of axons from the ipsilateral LOT ($M = 0.853 \pm 0.047$) compared to the contralateral LOT of the same animals ($M = 0.810 \pm 0.048$; $p < .0001$) and to normal controls ($M = 0.813 \pm 0.048$; $p < .001$), confirming thinner myelin sheaths in the ipsilateral LOT (Figure 7f,g). Second, an increase in the density of promyelinated axons was observed in both the LOT ipsilateral (4.26 ± 1.13 axons/100 $\mu m^2$) and contralateral (3.18 ± 0.74 axons/100 $\mu m^2$) to occlusion compared to P30 controls (2.99 ± 0.75axons/100$\mu m^2$). The density observed in experimental mice at P30 was similar to that recorded in unmanipulated mice at P20 (4.15 ± 0.42 axons/100 $\mu m^2$), potentially indicating that naris occlusion delayed the progression of myelination.

### 3.5.2 | Anterior commissure

The AC shared several characteristics with the LOT. For example, naris occlusion did not affect the density of myelinated axons (experimental $M = 114.30 \pm 30.63$ axons/100 $\mu m^2$; control $M = 117.11 \pm 31.27$ axons/100 $\mu m^2$; $t = 1.2$, $p = .14$; Figure 7a). Furthermore, myelin was significantly thinner in the AC of occluded animals (0.060 ± 0.02 μm) compared to age-matched controls (0.067 ± 0.03 μm; $p < .05$; Figure 7c). However, unlike the findings in the LOT, mean myelinated axon caliber was also significantly smaller in experimental animals (0.14 ± 0.01 μm) compared to controls (0.17 ± 0.03 μm; $U = 10.29$, $p = .001$). Therefore, it was appropriate to use g-ratios to determine whether the differences observed resulted from sampling variation or from an actual thinning of the myelin sheath. Mean g-ratios of myelinated axons in occluded animals (0.813 ± 0.24) did not differ from controls (0.83 ± 0.19; $t = 1.262$; $p = .21$), suggesting that unilateral naris occlusion does not affect myelin sheath thickness in the AC. Unlike the LOT, no differences in the number of promyelinated axons was found between experimental (24.12 ± 9.33 axons/100 $\mu m^2$) and control animals (20.93 ± 7.95 axons/100 $\mu m^2$).

## 4 | DISCUSSION

Few studies have examined myelination in the LOT and AC despite the fact that they are major forebrain white matter tracts and are conserved across the vertebrate lineage (Eisthen, 1997; Suárez et al., 2014). Each tract processes different aspects of the olfactory data stream. Odors detected by sensory neurons in the nose are translated into a topographic code in the OB. The LOT then transmits the information to the olfactory cortices where stimuli are identified and assigned into behavioral categories (Gire et al., 2013; Gottfried, 2010; Kadohisa & Wilson, 2006; Mori, 2014; Schwob & Price, 1984). The AC is involved in coordinating activity between the left and right cortices, allowing for localization of odor sources (Esquivelzeta-Rabell et al., 2017) and facilitating the interhemispheric transfer of stored memories (Fontaine et al., 2013; Kucharski & Hall, 1990, 1988; Kucharski et al., 1988).

The results presented above provide an opportunity to directly compare the two tracts on a number of dimensions (Table 2). First, the findings add substantial confirmation that the tracts differ in their patterns of development. It has been well established that the LOT originates very early compared to the rest of the forebrain (López-Mascaraque et al., 1996; Sato et al., 1998). Mitral cell axons exit the OB as early as E11.5 and begin to form the LOT by E13 (Walz et al., 2006), around the time that retinal ganglion cell axons begin forming the optic tract (Deiner et al., 1997), and before olfactory sensory neurons form synapses in the OB (Hinds & Hinds, 1976). Mitral cell projections separate into dorsal and ventral components of the LOT, and this rough topography can be seen as early as the day after birth (Walz et al., 2006). Prenatal development of the LOT allows for odor information to reach the ipsilateral cortex by birth, as it is crucial that olfactory pathways be established before suckling begins (Logan et al., 2012). Myelination of the LOT also occurs early. It is initiated around the same time as the optic chiasm and internal tracts of the cerebellum (P7) and within the CNS is only preceded by that of the spinal cord (Foran & Peterson, 1992). Axons first enter the AC much later than the LOT (E16), around the same time as the corpus callosum forms (Silver et al., 1982). The timing of myelination in the AC is also remarkably

similar to the corpus callosum. Myelinated axons appear in the corpus callosum at P11, the same day that they were first observed in the present study of the AC. Additionally, the corpus callosum begins a rapid phase of myelination around P14, which mirrors the results in the AC. (Figures 5 and 6) As the AC is involved in higher- order processing of olfactory information it appears to not be necessary for survival in neonates. In fact, AC transection does not affect performance on olfactory memory tasks until P12 in rats (Kucharski & Hall, 1990).

The study focused on examining patterns of postnatal development. Several approaches demonstrated conclusively that the time of myelination onset differs between the LOT and AC. Quantitative analyses of the expression of a number of markers for early-to-late stages of oligodendrocyte development indicated that precursor (PDGF+ and NG2+) populations decline earlier in the LOT than AC and markers for mature oligodendrocytes (CC1) and myelin sheaths (MBP) appeared later in the AC. EM was also used to quantify the number of promyelinated and myelinated axons as well as myelin thickness. Promyelinated axons were first encountered in the LOT at P7, but not until P11 in the AC. A large increase in the density and percentage of myelinated fibers occurred in the LOT between P9 and P13, while a similar increase did not occur in the AC until between P17 and P20.

It is important to note that both the LOT and AC are comprised of axons from different cell types, each of which could differ in their timing of myelination. For example, axons from two very different OB relay neurons form the LOT. Mitral cells are formed very early (E11–13 in the rat) and tufted cells arise later (E13–E18, Hinds, 1968). Mitral cell axons innervate broad regions of olfactory cortex while the axons of tufted cells are restricted to regions to the olfactory peduncle, including the AON and olfactory tubercle. Pyramidal cells from two regions, the AON and APC, enter the AC, and there is evidence that they are also not a homogeneous population (Kay & Brunjes, 2014). A similar pattern has been observed in the corpus callosum, in which homotopic and heterotopic projections develop on a different time course (Fenlon et al., 2017). Future studies should clarify the contributions of different cell types on the overall developmental patterns observed in the present findings in both the LOT and AC.

Second, the present findings demonstrate that there are notable organizational and morphological differences between the LOT and AC that can be seen across many ages (Table 2). For example, myelinated axon caliber was approximately 50% larger in the LOT than AC. A difference in axon size has been noted before (Brunjes, 2013). These observations suggest that the olfactory system has two processing streams: one for immediate odor processing (LOT) and one for slower subsequent processing (AC). The LOT also includes a much higher percentage of myelinated axons by P30 (84%) than the AC (23%; see also Livy et al., 1997; Sturrock, 1987). Myelin sheaths of LOT fibers are 2× thicker than that of the AC, which doubtlessly contributes to differences reported above in conduction velocity.

Third, the two tracts differ in their response to altered early experience. The proper formation of myelin sheaths is linked to efficient neuronal activity both in vivo and in vitro (Demerens et al., 1996), and it has been repeatedly demonstrated that early experience affects the rate and extent of myelination. For example, sensory deprivation decreases myelin thickness in the barrel cortex (Barrera et al., 2013) and social isolation has large effects on the development of myelin in the prefrontal cortex (Makinodan et al., 2012). Many studies have demonstrated that unilaterally reducing odor access by blocking air flow through one half of the nasal cavity in young pups causes profound changes in the development of the OB and olfactory cortices (Brunjes, 1994; Coppola, 2012). Naris closure, therefore, was used to examine if activity affects the development of these two tracts.

Substantial changes were observed in the LOT. Indeed, both the LOT ipsilateral and contralateral to occlusion exhibited both thinner myelin sheaths and an increased density of pro-myelinated cells at P30 compared to age-matched controls. Evidence did indicate, however, that the LOT on the occluded side was more affected as g-ratios were significantly larger. The findings are intriguing because unilateral naris closure has rarely been reported to affect the contralateral side. One possibility is that excessive stimulation resulting from the constant activation of the unoccluded nasal cavity might overdrive the ipsilateral OB and thus be a factor in the changes. Furthermore, in normal animals, the total amount and quality of olfactory stimulation should be roughly similar on both sides of the brain. Perhaps lifelong unbalanced stimulation changes developmental patterns in both the left and right hemispheres.

No consistent effects of occlusion were detected in the AC. While significantly thinner myelin sheaths were observed in experimental animals, the finding has to be interpreted in light of the fact that average axon caliber was also reduced. Several possibilities might explain these results. First, they may reflect sampling differences between groups. While no regional differences in axon caliber have been reported in the AC (Brunjes, 2013), it is possible that the random sampling methods employed provided proportionally more small caliber axons in the experimental group. This explanation seems possible as the g-ratios (the proportion of myelin relative to axon size) did not differ between groups: thus, when controlling for axon size, unilateral naris occlusion did not affect myelin thickness. However, it is also possible that naris occlusion decreases axon caliber. Alternatively, occlusion might preferentially affect larger-caliber axons (either by inhibiting the initiation of myelination or causing a shortening of internodes), thus resulting in a thinner overall population. Definitive evidence as to whether naris occlusion affects the AC will necessitate further study.

There are several explanations for why the LOT and AC might be differentially affected by unilateral naris occlusion. First, the LOT may be more sensitive to changes in afferent activity as it receives direct input from the ipsilateral OB. Second, differences could be more difficult to assess in the AC as (a) unlike the LOT it contains axons from both the manipulated and unmanipulated hemispheres, and (b) myelin sheaths in the AC of normal animals are already thinner than the LOT (Figure 6n). No difference in the number of myelinated axons or oligodendrocytes was found in either tract, supporting findings from other sensory systems that neuronal activity is important for initiation of myelination as well as regulation of sheath thickness and internodal length, but not for maintaining oligodendrocyte cell density or density of myelinated fibers (Barrera et al., 2013; Bercury and Macklin, 2015; Makinodan et al., 2012).

Taken together, the findings presented above indicate that the LOT and AC are particularly interesting and unique regions for studying myelination. Both tracts are compact, easily defined, and geographically separated yet are both contained in the small olfactory peduncle. Both exhibit considerable developmental differences, including the time of initial formation, functional state at birth, and rates of postnatal maturation. The two tracts have different spectrums of axons, including caliber and percentage myelinated. Furthermore, as both tracts carry sensory information, activity levels are relatively easy to manipulate. Interestingly, they carry different aspects of the olfactory data stream, and, as shown above, are differently affected by early changes in function. The present work substantially adds to previous findings of developmental and structural differences between the LOT and AC by providing the first direct comparison of myelination of these two olfactory system tracts (Table 2). The outlined differences between the LOT and the AC make the olfactory system a uniquely appropriate subject for studying the development of and factors affecting myelination.

## CONFLICT OF INTEREST

The authors have no conflicts of interest.

## ORCID

*P. C. Brunjes* http://orcid.org/0000-0003-4306-1543

## REFERENCES

Aggarwal, S., Yurlova, L., & Simons, M. (2011). Central nervous system myelin: Structure, synthesis, and assembly. *Trends in Cell Biology*, *21*(10), 585–593.

Al-Mayhani, M. T. F., Grenfell, R., Narita, M., Piccirillo, S., Kenney-Herbert, E., Fawcett, J. W., & Watts, C. (2011). NG2 expression in glioblastoma identifies an actively proliferating population with an aggressive molecular signature. *Neuro-oncology*, *13*(8), 830–845.

Asou, H., Hamada, K., Miyazaki, T., Sakota, T., Hayashi, K., Takeda, Y., … Uyemura, K. (1995). CNS myelinogenesis in vitro: Time course and pattern of rat oligodendrocyte development. *Journal of Neuroscience Research*, *40*(4), 519–534.

Barrera, K., Chu, P., Abramowitz, J., Steger, R., Ramos, R. L., & Brumberg, J. C. (2013). Organization of myelin in the mouse somatosensory barrel cortex and the effects of sensory deprivation. *Developmental Neurobiology*, *73*(4), 297–314.

Baumann, N., & Pham-Dinh, D. (2001). Biology of oligodendrocyte and myelin in the mammalian central nervous system. *Physiological Reviews*, *81*(2), 871–927.

Bercury, K. K., & Macklin, W. B. (2015). Dynamics and mechanisms of CNS myelination. *Developmental Cell*, *32*(4), 447–458.

Bergsten, E., Uutela, M., Li, X., Pietras, K., Östman, A., Heldin, C. H., … Eriksson, U. (2001). PDGF-D is a specific, protease-activated ligand for the PDGF [beta]-receptor. *Nature Cell Biology*, *3*(5), 512.

Bhat, R. V., Axt, K. J., Fosnaugh, J. S., Smith, K. J., Johnson, K. A., Hill, D. E., … Baraban, J. M. (1996). Expression of the APC tumor suppressor protein in oligodendroglia. *Glia*, *17*(2), 169–174.

Blanchart, A., De Carlos, J., & Lopez-Mascaraque, L. (2006). Time frame of mitral cell development in the mice olfactory bulb. *Journal of Comparative Neurology*, *496*(4), 529–543.

Brunjes, P. (1994). Unilateral naris closure and olfactory system development. *Brain Research Reviews*, *19*(1), 146–160.

Brunjes, P. (2013). The mouse olfactory peduncle. 2. The anterior limb of the anterior commissure. *Frontiers in Neuroanatomy*, *6*, 51.

Brunjes, P., Collins, L., Osterberg, S., & Phillips, A. (2014). The mouse olfactory peduncle. 3. Development of neurons, glia, and centrifugal afferents. *Frontiers in Neuroanatomy*, *8*, 44.

Brunjes, P. C., Kay, R. B., & Arrivillaga, J. P. (2011). The mouse olfactory peduncle. *J Comp Neurol*, *519*, 2870–2886.

Calver, A. R., Hall, A. C., Yu, W. P., Walsh, F. S., Heath, J. K., Betsholtz, C., & Richardson, W. D. (1998). Oligodendrocyte population dynamics and the role of PDGF in vivo. *Neuron*, *20*(5), 869–882.

Chomiak, T., & Hu, B. (2009). What is the optimal value of the g-ratio for myelinated fibers in the rat CNS? A theoretical approach. *PloS One*, *4*(11), e7754.

Coppola, D. (2012). Studies of olfactory system neural plasticity: The contribution of the unilateral naris occlusion technique. *Neural Plasticity*, *2012*, 14.

Dawson, M. R., Polito, A., Levine, J. M., & Reynolds, R. (2003). NG2-expressing glial progenitor cells: an abundant and widespread population of cycling cells in the adult rat CNS. *Molecular and Cellular Neuroscience*, *24*(2), 476–488.

Deiner, M. S., Kennedy, T. E., Fazeli, A., Serafini, T., Tessier-Lavigne, M., & Sretavan, D. W. (1997). Netrin-1 and DCC mediate axon guidance locally at the optic disc: Loss of function leads to optic nerve hypoplasia. *Neuron*, *19*(3), 575–589.

Demerens, C., Stankoff, B., Logak, M., Anglade, P., Allinquant, B., Couraud, F., … Lubetzki, C. (1996). Induction of myelination in the central nervous system by electrical activity. *Proceedings of the National Academy of Sciences*, *93*(18), 9887–9892.

Downes, N., & Mullins, P. (2014). The development of myelin in the brain of the juvenile rat. *Toxicologic Pathology*, *42*(5), 913–922.

Eisthen, H. L. (1997). Evolution of vertebrate olfactory systems. *Brain, Behavior and Evolution*, *50*(4), 222–233.

Etxeberria, A., Mangin, J. M., Aguirre, A., & Gallo, V. (2010). Adult-born SVZ progenitors receive transient synapses during remyelination in corpus callosum. *Nature Neuroscience*, *13*(3), 287–289.

Fenlon, L. R., Suárez, R., & Richards, L. J. (2017). The anatomy, organisation and development of contralateral callosal projections of the mouse somatosensory cortex. *Brain and Neuroscience Advances*, *1*, https://doi.org/10.1177/2398212817694888.

Fontaine, C. J., Harley, C. W., & Yuan, Q. (2013). Lateralized odor preference training in rat pups reveals an enhanced network response in anterior piriform cortex to olfactory input that parallels extended memory. *Journal of Neuroscience*, *33*(38), 15126–15131.

Foran, D. R., & Peterson, A. C. (1992). Myelin acquisition in the central nervous system of the mouse revealed by an MBP-Lac Z transgene. *Journal of Neuroscience*, *12*, 4890–4890.

Fruttiger, M., Karlsson, L., Hall, A. C., Abramsson, A., Calver, A. R., Bostrom, H., Willetts, K., … Richardson, W. D. (1999). Defective oligodendrocyte development and severe hypomyelination in PDGF-A knockout mice. *Development*, *126*(3), 457–467.

Gilbertson, D. G., Duff, M. E., West, J. W., Kelly, J. D., Sheppard, P. O., Hofstrand, P. D., … Hart, C. E. (2001). Platelet-derived growth factor C (PDGF-C), a novel growth factor that binds to PDGF α and β receptor. *Journal of Biological Chemistry*, *276*(29), 27406–27414.

Gire, D. H., Restrepo, D., Sejnowski, T. J., Greer, C., De Carlos, J. A., & Lopez-Mascaraque, L. (2013). Temporal processing in the olfactory system: Can we see a smell? *Neuron*, *78*(3), 416–432.

Gottfried, J. A. (2010). Central mechanisms of odour object perception. *Nature Reviews Neuroscience*, *11*(9), 628.

Gottlieb, A., Keydar, I. K., & Epstein, H. T. (1977). Rodent brain growth stages: An analytical review. *Biology of the Neonate*, *32*(3–4), 166–176.

Grishchuk, Y., Peña, K. A., Coblentz, J., King, V. E., Humphrey, D. M., Wang, S. L., … Laugenhaupt, S. A. (2015). Impaired myelination and reduced brain ferric iron in the mouse model of mucolipidosis IV. *Disease Models & Mechanisms*, *8*(12), 1591–1601.

Guillery, R. W., & Herrup, K. (1997). Quantification without pontification: Choosing a method for counting objects in sectioned tissues. *Journal of Comparative Neurology*, *386*(1), 2–7.

Haberly, L. B., & Price, J. L. (1978). Association and commissural fiber systems of the olfactory cortex of the rat. II. Systems originating in the olfactory peduncle. *J Comp Neurol*, *178*, 781–808.

Hinds, J. W. (1968). Autoradiographic study of histogenesis in the mouse olfactory bulb. I. Time of origin of neurons and neuroglia. *Journal of Comparative Neurology*, *134*(3), 287–304.

Hinds, J. W., & Hinds, P. L. (1976). Synapse formation in the mouse olfactory bulb. Quantitative studies. *Journal of Comparative Neurology*, *169*(1), 15–40.

Jakovcevski, I., Filipovic, R., Mo, Z., Rakic, S., & Zecevic, N. (2009). Oligodendrocyte development and the onset of myelination in the human fetal brain. *Frontiers in Neuroanatomy*, *3*, 5.

Jiao, Y., Sun, Z., Lee, T., Fusco, F. R., Kimble, T. D., Meade, C. A., … Reiner, A. (1999). A simple and sensitive antigen retrieval method for free-floating and slide-mounted tissue sections. *Journal of Neuroscience Methods*, *93*(2), 149–162.

Kadohisa, M., & Wilson, D. A. (2006). Separate encoding of identity and similarity of complex familiar odors in piriform cortex. *Proceedings of the National Academy of Sciences*, *103*(41), 15206–15211.

Kay, R. B., & Brunjes, P. C. (2014). Diversity among principal and GABAergic neurons of the anterior olfactory nucleus. *Frontiers in Cellular Neuroscience*, *8*, 111. https://doi.org/10.3389/fncel.2014.00111

Kucharski, D., Burka, N., & Hall, W. G. (1990). The anterior limb of the anterior commissure is an access route to contralateral stored olfactory preference memories. *Psychobiology*, *18*(2), 195–204.

Kucharski, D., & Hall, W. G. (1987). New routes to early memories. *Science (New York, N.Y.)*, *238*(4828), 786–788.

Kucharski, D., & Hall, W. G. (1988). Developmental change in the access to olfactory memories. *Behavioral Neuroscience*, *102*(3), 340–348.

Livy, D. J., Schalomon, P. M., Roy, M., Zacharias, M. C., Pimenta, J., Lent, R., & Wahlsten, D. (1997). Increased axon number in the anterior commissure of mice lacking a corpus callosum. *Experimental Neurology*, *146*(2), 491–501.

Logan, D., Brunet, L., Webb, W., Cutforth, T., Ngai, J., & Stowers, L. (2012). Learned recognition of maternal signature odors mediates the first suckling episode in mice. *Current Biology*, *22*(21), 1998–2007.

López-Mascaraque, L., De Carlos, J. A., & Valverde, F. (1996). Early onset of the rat olfactory bulb projections. *Neuroscience*, *70*, 255–266.

Makinodan, M., Rosen, K., Ito, S., & Corfas, G. (2012). A critical period for social experience-dependent oligodendrocyte maturation and myelination. *Science*, *337*, 1357–1360.

Mateo, J., van den Berg, D., Haeussler, M., Drechsel, D., Gaber, Z., Castro, D., … Martynoga, B. (2015). Characterization of the neural stem cell gene regulatory network identifies OLIG2 as a multifunctional regulator of self-renewal. *Genome Research*, *25*(1), 41–56.

Matoba, K., Muramatsu, R., & Yamashita, T. (2017). Leptin sustains spontaneous remyelination in the adult central nervous system. *Scientific Reports*, *7*, 40397.

Medina, E. (1993). Demyelinating and dysmyelinating diseases. *Rivista Di Neuroradiologia*, *6*(2), 33–38.

Mori, K. (2014). *The olfactory system: From odor molecules to motivational behaviors*. Tokyo: Springer.

Ness, J. K., Valentino, M., McIver, S. R., & Goldberg, M. P. (2005). Identification of oligodendrocytes in experimental disease models. *Glia*, *50*(4), 321–328.

Nishiyama, A., Komitova, M., Suzuki, R., & Zhu, X. (2009). Polydendrocytes (NG2 cells): multifunctional cells with lineage plasticity. *Nature Reviews Neuroscience*, *10*(1), 9.

Nishiyama, A., Lin, X., Giese, N., Heldin, C., & Stallcup, W. (1996). Co-localization of NG2 proteoglycan and PDGF α-receptor on O2A progenitor cells in the developing rat brain. *Journal of Neuroscience Research*, *43*(3), 299–314.

Nishiyama, A., Watanabe, M., Yang, Z., & Bu, J. (2002). Identity, distribution, and development of polydendrocytes: NG2-expressing glial cells. *Journal of Neurocytology*, *31*(6–7), 437.

Padiath, Q. S., Saigoh, K., Schiffmann, R., Asahara, H., Yamada, T., Koeppen, A., … Ying-Hui, F. (2006). Lamin B1 duplications cause autosomal dominant leukodystrophy. *Nature Genetics*, *38*(10), 1114.

Pringle, N. P., Mudhar, H. S., Collarini, E. J., & Richardson, W. D. (1992). PDGF receptors in the rat CNS: During late neurogenesis, PDGF alpha-receptor expression appears to be restricted to glial cells of the oligodendrocyte lineage. *Development*, *115*(2), 535–551.

Rabell, J. E., Mutlu, K., Noutel, J., del Olmo, P. M., & Haesler, S. (2017). Spontaneous rapid odor source localization behavior requires interhemispheric communication. *Current Biology*, *27*(10), 1542–1548.

Rasband, W. (1997). *ImageJ*. Bethesda, MD: US National Institutes of Health. Available from http://rsb.info.nih.gov/ij

Rivers, L., Young, K., Rizzi, M., Jamen, F., Psachoulia, K., Wade, A., … Richardson, W. (2008). PDGFRA/NG2 glia generate myelinating oligodendrocytes and piriform projection neurons in adult mice. *Nature Neuroscience*, *11*(12), 1392–1401.

Rosselli-Austin, L., & Altman, J. (1979). The postnatal development of the main olfactory bulb of the rat. *Journal of Developmental Physiology*, *1*(4), 295–313.

Rushton, W. (1951). A theory of the effects of fibre size in medullated nerve. *Journal of Physiology*, *115*(1), 101–122.

Sampaio, R., & Truwit, C. (2001). Myelination in the developing human brain. In C. A. Nelson and M. Luciana (Eds.), *Handbook of developmental cognitive neuroscience* (pp. 35–44). Cambridge, MA: MIT Press.

Sato, Y., Hirata, T., Ogawa, M., & Fujisawa, H. (1998). Requirement for early-generated neurons recognized by monoclonal antibody lot1 in the formation of lateral olfactory tract. *Journal of Neuroscience*, *18*, 7800–7810.

Schmued, L. C. (1990). A rapid, sensitive histochemical stain for myelin in frozen brain sections. *Journal of Histochemistry and Cytochemistry: Official Journal of the Histochemistry Society*, *38*, 717–720.

Schwob, J., & Price, J. (1984). The development of axonal connections in the central olfactory system of rats. *Journal of Comparative Neurology*, *223*(2), 177–202.

Shearer, M., Niclou, S., Brown, D., Asher, R., Holtmaat, A., Levine, J., … Fawcett, J. (2003). The astrocyte/meningeal cell interface is a barrier to neurite outgrowth which can be overcome by manipulation of inhibitory molecules or axonal signalling pathways. *Molecular and Cellular Neurosciences*, *24*(4), 913–925.

Shiota, C., Miura, M., & Mikoshiba, K. (1989). Developmental profile and differential localization of mRNAs of myelin proteins (MBP and PLP) in oligodendrocytes in the brain and in culture. *Developmental Brain Research*, *45*(1), 83–94.

Silver, J., Lorenz, S. E., Wahlsten, D., & Coughlin, J. (1982). Axonal guidance during development of the great cerebral commissures: Descriptive

and experimental studies, in vivo, on the role of preformed glial pathways. *Journal of Comparative Neurology*, *210*(1), 10–29.

Smith, K., Johnson, K., Bryan, T., Hill, D., Markowitz, S., Willson, J., … Kinzler, K. (1993). The APC gene product in normal and tumor cells. *Proceedings of the National Academy of Sciences*, *90*(7), 2846–2850.

Stanton, G. B., Kohler, S. J., Boklweski, J., Cameron, J. L., & Greenough, W. T. (2015). Cytogenesis in the adult monkey motor cortex: Perivascular NG2 cells are the major adult born cell type. *Journal of Comparative Neurology*, *523*(6), 849–868.

Sturrock, R. R. (1976). Development of the mouse anterior commissure. Part I. A comparison of myelination in the anterior and posterior limbs of the anterior commissure of the mouse brain. *Anatomia, Histologia, Embryologia: Journal of Veterinary Medicine Series C*, *5*, 54–67.

Sturrock, R. R. (1987). Age-related changes in the number of myelinated axons and glial cells in the anterior and posterior limbs of the mouse anterior commissure. *Anatomia, Histologia, Embryologia: Journal of Veterinary Medicine Series C*, *150*, 111.

Suárez, R., Gobius, I., & Richards, L. J. (2014). Evolution and development of interhemispheric connections in the vertebrate forebrain. *Frontiers in Human Neuroscience*, *8*, 497.

Takebayashi, H., Nabeshima, Y., Yoshida, S., Chisaka, O., Ikenaka, K., & Nabeshima, Y. I. (2002). The basic helix-loop-helix factor olig2 is essential for the development of motoneuron and oligodendrocyte lineages. *Current Biology*, *12*(13), 1157–1163.

Wahl, S., McLane, L., Bercury, K., Macklin, W., & Wood, T. (2014). Mammalian target of rapamycin promotes oligodendrocyte differentiation, initiation and extent of CNS myelination. *Journal of Neuroscience*, *34*(13), 4453–4465.

Walz, A., Omura, M., & Mombaerts, P. (2006). Development and topography of the lateral olfactory tract in the mouse: Imaging by genetically encoded and injected fluorescent markers. *Journal of Neurobiology*, *6*(8), 835–846.

Watson, R., DeSesso, J., Hurtt, M., & Cappon, G. (2006). Postnatal growth and morphological development of the brain: A species comparison. *Birth Defects Research Part B: Developmental and Reproductive Toxicology*, *77*(5), 471–484.

**How to cite this article:** Collins LN, Hill DL, Brunjes PC. Myelination of the developing lateral olfactory tract and anterior commissure. *J Comp Neurol*. 2018;526:1843–1858. https://doi.org/10.1002/cne.24452